Bulk and wetting phenomena in a colloidal mixture of hard spheres and platelets

L. Harnau and S. Dietrich
Max-Planck-Institut für Metallforschung, Heisenbergstrasse 3, D-70569 Stuttgart, Germany
and Institut für Theoretische und Angewandte Physik, Universität Stuttgart, Pfaffenwaldring 57, D-70569 Stuttgart, Germany
(Received 27 August 2004; revised manuscript received 28 October 2004; published 14 January 2005)

Density functional theory is used to study binary colloidal fluids consisting of hard spheres and thin platelets in their bulk and near a planar hard wall. This system exhibits liquid-liquid coexistence of a phase that is rich in spheres (poor in platelets) and a phase that is poor in spheres (rich in platelets). For the mixture near a planar hard wall, we find that the phase rich in spheres wets the wall completely upon approaching the liquid demixing binodal from the sphere-poor phase, provided the concentration of the platelets is smaller than a threshold value which marks a first-order wetting transition at coexistence. No layering transitions are found, in contrast to recent studies on binary mixtures of spheres and nonadsorbing polymers or thin hard rods.

DOI: 10.1103/PhysRevE.71.011504 PACS number(s): 64.70.Ja, 68.08.Bc, 82.70.Dd

I. INTRODUCTION

Rich bulk phase diagrams involving colloidal gas, liquid, and solid phases are found when nonadsorbing polymers or hard rodlike colloids are added as depletion agents to suspensions of colloidal spheres [1,2]. The chemical potential of the polymers or rods, with which one can tune their concentration, plays a role equivalent to that of the inverse temperature for a simple one-component substance characterized by a soft pair potential. Moreover, it has been shown theoretically [3,4] and by computer simulation [5] that entropic depletion mechanisms lead to interesting wetting phenomena and to a rich surface phase behavior in colloidal mixtures of spheres and noninteracting polymers or rods. A wetting transition and layering transitions have been found when the mixtures are exposed to a hard wall.

Recently the depletion potential between two hard spheres due to the presence of hard-disk-like colloids has been investigated [6–9]. Subsequently it has been shown within a free-volume theory that depletion-induced phase separation in a colloidal sphere-platelet mixture should occur at low platelet concentrations in systems now experimentally available [10]. In view of the importance of such suspensions in biomedicine [11] and geophysics [12] we investigate in the present paper bulk and wetting phenomena of sphere-platelet mixtures using density functional theory. We demonstrate that the geometry-based density functional theory developed for binary mixture of hard spheres and thin rods [13–16] can be consistently extended to the problem of hard spheres mixed with a low concentration of thin hard platelets (Sec. II). Moreover, we study the bulk phase diagram (Sec. III) and the wetting of the mixture at a planar hard wall by considering the platelets as thin and noninteracting regarding their mutual interactions (Sec. IV). Our study provides a direct comparison of the bulk and wetting properties of binary sphere-platelet and sphere-rod mixtures.

II. DENSITY FUNCTIONAL AND FUNDAMENTAL MEASURE THEORY

We consider a binary mixture of hard spheres and thin circular platelets of radius R_s and R_p, respectively. The number density of the centers of mass of the platelets at a point $\mathbf{r}$ with an orientation $\omega_p=(\theta_p,\phi_p)$ of the normal of the platelets is denoted by $\rho_p(\mathbf{r},\omega_p)$ while $\rho_s(\mathbf{r})$ is the center-of-mass number density of the spheres. The equilibrium density profiles of the inhomogeneous mixture under the influence of external potentials $V_{ext,s}(\mathbf{r})$ and $V_{ext,p}(\mathbf{r},\omega_p)$ minimize the grand potential functional

$$\begin{aligned}\Omega[\rho_s,\rho_p] &= \int d^3r\, \rho_s(\mathbf{r})(k_BT\{\ln[\Lambda_s^3\rho_s(\mathbf{r})]-1\}-\mu_s+V_{ext,s}(\mathbf{r})) \\ &+\frac{1}{4\pi}\int d^3r\, d\omega_p \rho_p(\mathbf{r},\omega_p)(k_BT\{\ln[\Lambda_p^3\rho_p(\mathbf{r},\omega_p)]-1\} \\ &-\mu_p+V_{ext,p}(\mathbf{r},\omega_p))+F_{ex}[\rho_s,\rho_p], \end{aligned} \tag{1}$$

where Λ_s,Λ_p are the thermal de Broglie wavelengths and μ_s,μ_p are the chemical potentials of the spheres and platelets, respectively. The spatial integrals run over the volume V that is accessible to the centers of the particles and $\int d\omega = \int_0^\pi d\theta \int_0^{2\pi} d\phi$. The excess free energy functional is obtained by integrating over an excess free energy density,

$$F_{ex}[\rho_s,\rho_p]=\frac{k_BT}{4\pi}\int d^3r\, d\omega_p \Phi(\{n_\nu^{(s)},\mathbf{n}_i^{(s)},n_\tau^{(p)},n^{(sp)}\}), \tag{2}$$

where $\nu=0,1,2,3$, $i=1,2$, and $\tau=0,1,2$. In Eq. (2) the spatial and angular arguments of the weighted densities $n_\nu^{(s)}$, $\mathbf{n}_i^{(s)}$, $n_\tau^{(p)}$, and $n^{(sp)}$ are suppressed in the notation. Here we use the following decomposition of the excess free energy density Φ:

$$\Phi=\Phi_s+\Phi_{sp}, \tag{3}$$

with [17]

$$\begin{aligned}\Phi_s &= -n_0^{(s)}\ln(1-n_3^{(s)})+\frac{n_1^{(s)}n_2^{(s)}-\mathbf{n}_1^{(s)}\cdot\mathbf{n}_2^{(s)}}{1-n_3^{(s)}} \\ &+\frac{(n_2^{(s)})^3-3n_2^{(s)}(\mathbf{n}_2^{(s)})^2}{24\pi(1-n_3^{(s)})^2}, \end{aligned} \tag{4}$$

and a new contribution

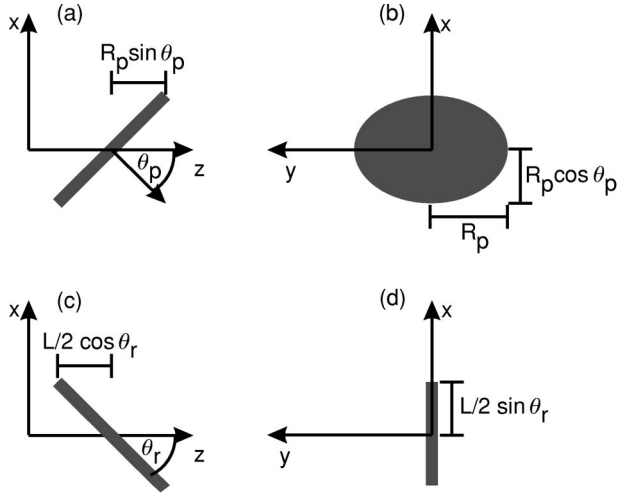

FIG. 1. Geometries relevant for the determination of the weight functions [Eqs. (15), (16), and (19)–(21)] for thin circular platelets of radius R_p (a),(b) and thin rods of length L (c),(d). The angle between the normal of a platelet and the z axis is denoted by θ_p while the angle θ_r characterizes the orientation of a rod with respect to the z axis. Only the projections of the platelets and rods on the planes of the figures are shown.

$$\Phi_{sp} = -n_0^{(p)} \ln(1-n_3^{(s)}) + \frac{n_1^{(p)} n^{(sp)} + n_1^{(s)} n_2^{(p)}}{1-n_3^{(s)}} + \frac{\pi n_2^{(p)} (n_2^{(s)})^2}{64(1-n_3^{(s)})^2}. \tag{5}$$

Φ_s is the original Rosenfeld excess free energy density [17] for a pure hard sphere fluid. (For the subtle issue of the range of validity of the Rosenfeld functional at high densities, see Refs. [18,19].) Φ_{sp} takes sphere-platelet interactions into account up to first order in the number density of the platelets (see discussion below). There is no contribution Φ_{pp} to the excess free energy Φ in Eq. (4) because the low concentration of platelets allows us to treat them as noninteracting particles regarding their mutual interactions. In the present application of density functional theory we concentrate on ordering effects induced by a planar hard wall such that the resulting density profile of the spheres depends on a single spatial variable z in the direction normal to the wall. Hence $\rho_s(\mathbf{r}) = \rho_s(z)$ apart from possible surface freezing at high densities. Moreover, we assume invariance with respect to rotations around the z axis by an angle ϕ_p, so that $\rho_p(\mathbf{r}, \omega_p) = \rho_p(z, \theta_p)$, where θ_p is the angle between the normal of a platelet and the z axis (see Fig. 1). In this planar geometry the weighted densities are given by

$$n_\nu^{(s)}(z) = \rho_s(z) * w_\nu^{(s)}(z), \tag{6}$$

$$\mathbf{n}_i^{(s)}(z) = \rho_s(z) * \mathbf{w}_i^{(s)}(z), \tag{7}$$

$$n_\tau^{(p)}(z, \theta_p) = \rho_p(z, \theta_p) * w_\tau^{(p)}(z, \theta_p), \tag{8}$$

$$n^{(sp)}(z, \theta_p) = \rho_s(z) * w^{(sp)}(z, \theta_p), \tag{9}$$

where the asterisk $*$ denotes the spatial convolution: $g(z)*h(z) = \int dz_1 g(z_1) h(z - z_1) \equiv g*h$. Note that $n_\nu^{(s)}$, $\mathbf{n}_i^{(s)}$, and $n_\tau^{(p)}$ are weighted densities which involve only variables of either species, while $n^{(sp)}$ is a convolution of the sphere density with an orientation-dependent weight function, combining characteristics of both species. The weight functions of the Rosenfeld excess free energy density read

$$w_0^{(s)}(z) = \frac{\Theta(R_s - |z|)}{2R_s}, \tag{10}$$

$$w_1^{(s)}(z) = \frac{\Theta(R_s - |z|)}{2} = \frac{w_2^{(s)}(z)}{4\pi R_s}, \tag{11}$$

$$w_3^{(s)}(z) = \pi(R_s^2 - z^2)\Theta(R_s - |z|), \tag{12}$$

$$\mathbf{w}_1^{(s)}(z) = \frac{z\Theta(R_s - |z|)\mathbf{e}_z}{2R_s} = \frac{\mathbf{w}_2^{(s)}(z)}{4\pi R_s}, \tag{13}$$

where $\mathbf{e}_z$ is the unit vector pointing along the z axis and $\Theta(z)$ is the Heaviside step function. The integral of the Mayer function $f_{ss}(x,y,z)$ of the interaction potential between two hard spheres is obtained through

$$l_{ss}(z) = -\int_{-\infty}^{\infty} dx \int_{-\infty}^{\infty} dy\, f_{ss}(x,y,z) = 2(w_0^{(s)} * w_3^{(s)} + w_1^{(s)} * w_2^{(s)} - \mathbf{w}_1^{(s)} * \mathbf{w}_2^{(s)}). \tag{14}$$

The Mayer function equals -1 if the spheres intersect or touch each other and is zero otherwise. The remaining weight functions can be expressed as (see the Appendix for details)

$$w_0^{(p)}(z, \theta_p) = \frac{\theta(R_p \sin\theta_p - |z|)}{4R_p \sin\theta_p}, \tag{15}$$

$$w_1^{(p)}(z, \theta_p) = \frac{\pi\Theta(R_p \sin\theta_p - |z|)}{8 \sin\theta_p} = \frac{w_2^{(p)}(z, \theta_p)}{8R_p}, \tag{16}$$

and

$$w^{(sp)}(z, \theta_p) = 8\Theta(R_s \cos\theta_p - |z|)\sqrt{R_s^2 \cos^2\theta_p - z^2} + \Theta(R_s - |z|) v^{(sp)}(z, \theta_p) \sin\theta_p, \tag{17}$$

where the function $v^{(sp)}(z, \theta_p)$ is determined such that the integral of the Mayer function $f_{sp}(x,y,z,\omega_p)$ of the interaction potential between a hard sphere and a thin platelet is generated through

$$l_{sp}(z, \theta_p) = -\int_{-\infty}^{\infty} dx \int_{-\infty}^{\infty} dy\, f_{sp}(x,y,z,\omega_p) = w_0^{(p)} * w_3^{(s)} + w_1^{(p)} * w^{(sp)} + w_2^{(p)} * w_1^{(s)}, \tag{18}$$

where $l_{sp}(z, \theta_p)$ is independent of the azimuthal angle ϕ_p due to rotational symmetry. Equations (1)–(18) completely

specify the density functional theory for the system under consideration.

Before studying the binary mixture of spheres and thin platelets in the bulk and near a hard wall it is instructive to compare the fundamental measure theory with the one that has been developed recently for a mixture of hard spheres and thin rods [13–16]. For thin rods of length L the weight functions corresponding to Eqs. (15)–(17) are given by

$$w_0^{(r)}(z,\theta_r) = \frac{\delta((L/2)\cos\theta_r - |z|)}{2}, \tag{19}$$

$$w_1^{(r)}(z,\theta_r) = \frac{\Theta((L/2)\cos\theta_r - |z|)}{4\cos\theta_r}, \tag{20}$$

$$w_2^{(r)}(z,\theta_r) = 0, \tag{21}$$

and

$$w^{(sr)}(z,\theta_r) = 8\Theta(R_s\sin\theta_r - |z|)\sqrt{R_s^2\sin^2\theta_r - z^2} + \Theta(R_s - |z|)v^{(sr)}(z,\theta_r)\cos\theta_r, \tag{22}$$

where the function $v^{(sr)}(z,\theta_r)$ is determined such that the integral of the Mayer function $f_{sr}(x,y,z,\omega_r)$ of the interaction potential between a hard sphere and a thin rod is generated through

$$l_{sp}(z,\theta_r) = -\int_{-\infty}^{\infty}dx\int_{-\infty}^{\infty}dy\, f_{sr}(x,y,z,\omega_r) = w_0^{(r)} * w_3^{(s)} + w_1^{(r)} * w^{(sr)}, \tag{23}$$

where $l_{sr}(z,\theta_r)$ is independent of the azimuthal angle ϕ_r due to rotational symmetry. Here θ_r is the angle between the rod and the z axis (see Fig. 1). The weight functions are linked with a geometrical representation of the particles which is given in terms of fundamental measures defined as $\zeta_\lambda^{(j)} = \int dz\, w_\lambda^{(j)}$, where $j = s,p,r$ labels the species, and $\lambda = 0,1,2,3$ corresponds to the Euler characteristic, integral mean curvature, surface, and volume [20] of the particles. For spheres $\zeta_0^{(s)} = 1$, $\zeta_1^{(s)} = R_s$, $\zeta_2^{(s)} = 4\pi R_s^2$, and $\zeta_3^{(s)} = 4\pi R_s^3/3$, whereas for thin platelets the volume is very small and $\zeta_0^{(p)} = 1$, $\zeta_1^{(p)} = \pi R_p/4$, and $\zeta_2^{(p)} = 2\pi R_p^2$. In the case of thin rods both the volume and the surface area are very small and $\zeta_0^{(r)} = 1$, $\zeta_1^{(r)} = L/4$. For comparison we note that the integral mean curvature of a particle can be obtained from the general relation $\zeta_1 = \int d\sigma(1/R_1 + 1/R_2)/(8\pi)$, where R_1 and R_2 are the principle radii of curvature at the point σ on the surface and $d\sigma$ is a surface element. The evaluation of this integral is trivial for thin rods and is documented for thin platelets in the appendix of Ref. [21].

From their side view, platelets may be regarded as rods [see Figs. 1(a) and 1(c)] and from their top view (in the direction of the normal to face) as two-dimensional spheres. Therefore the functional forms of the weight functions $w_0^{(p)}(z)$, $w_0^{(r)}(z)$ [Eqs. (15) and (19)] and $w_1^{(p)}(z)$, $w_1^{(r)}(z)$ [Eqs. (16) and (20)] are similar, while the weight function $w_2^{(p)}(z)$ [Eq. (16)] takes into account the surface of the platelets [see Fig. 1(b)].

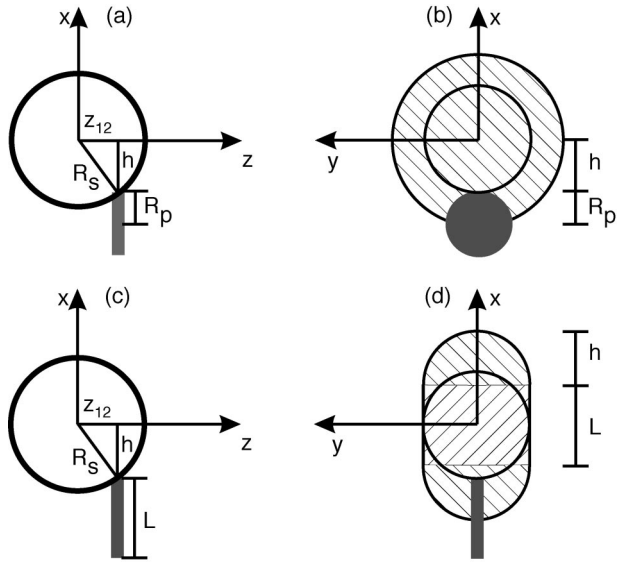

FIG. 2. Illustrations of the steric interactions of hard spheres with thin hard platelets and rods. (a) [(c)] Schematic side view of a sphere of radius R_s and a platelet of radius R_p (rod of length L). The normal of the platelet is parallel to the z axis while the rod is oriented parallel to the x axis. Only the projections of the particles on the planes of the figures are shown. (b) [(d)] Due to the steric interaction, the center of mass of the platelet (rod) is excluded from the hatched region surrounding the sphere in the x-y plane. Here the planes of the figures are located at $z = z_{12}$. From these figures the area $A_{sp}(z_{12}) = \pi(h+R_p)^2$ $[A_{sr}(z_{12}) = \pi h^2 + 2Lh]$ with $h = \sqrt{R_s^2 - z_{12}^2}$ can be inferred [see Eq. (25) Eq. (27)].

In order to express the integral of the sphere-platelet and sphere-rod Mayer functions [Eqs. (18) and (23)] in terms of spatial convolution decompositions, additional weight functions $w^{(sp)}(z,\theta_p)$ and $w^{(sr)}(z,\theta_r)$ have to be introduced. These weight functions contain information about both species of the binary mixtures. We analyze the cases $\theta_p = 0$ and $\theta_r = \pi/2$ in more detail. In these limits the weight functions reduce to $w^{(sp)}(z,\theta_p = 0) = w^{(sr)}(z,\theta_r = \pi/2) = 8\sqrt{R_s^2 - z^2}\Theta(R_s - |z|)$. Figure 2 displays schematic illustrations of the support of the integral of the sphere-platelet and sphere-rod Mayer functions which can be calculated analytically from Eqs. (18) and (23):

$$l_{sp}(z,\theta_p = 0) = A_{sp}(z)\Theta(R_s - |z|), \tag{24}$$

$$A_{sp}(z) = \pi(\sqrt{R_s^2 - z^2} + R_p)^2, \tag{25}$$

and

$$l_{sr}\left(z,\theta_r = \frac{\pi}{2}\right) = A_{sr}(z)\Theta(R_s - |z|), \tag{26}$$

$$A_{sr}(z) = \pi(R_s^2 - z^2) + 2L\sqrt{R_s^2 - z^2}. \tag{27}$$

Due to the steric interaction, the center of mass of a platelet (rod) is excluded from an area in the x-y plane of size

$A_{sp}(z_{12})$ $[A_{sr}(z_{12})]$ surrounding a sphere, where z_{12} is the distance along the z axis between the center of mass of the platelet (rod) and the sphere. Moreover it is apparent from the figure that the radius $\sqrt{R_s^2-z^2}$ and hence the weight function $w^{(sp)}(z,0)$ $[w^{(sr)}(z,\pi/2)]$ are characteristic of how a sphere looks from the viewpoint of a platelet (rod).

III. BULK PHASE DIAGRAM

Based on the density functional given by Eqs. (1)–(18) and as a prerequisite for our wall-liquid interface study we first study the homogeneous bulk fluid with $V_{ext,s}(\mathbf{r})=0$ and $V_{ext,p}(\mathbf{r},\omega_p)=0$ in a macroscopic volume V. In this case the equilibrium density profiles are constant $[\rho_s(\mathbf{r})=\rho_s$ and $\rho_p(\mathbf{r},\omega_p)=\rho_p]$ and the Euler-Lagrange equations resulting from the stationary conditions are given by $\partial\Omega[\rho_s,\rho_p]/\partial\rho_s=0$ and $\partial\Omega[\rho_s,\rho_p]/\partial\rho_p=0$. In the present study we restrict our attention to platelet number densities $\rho_p R_p^3 \leqslant 0.2$ for which the pure platelet fluid and also the mixture are in the isotropic phase and hence ρ_s is independent of the orientation of the platelets. For comparison, the isotropic-nematic phase transition of the pure platelet fluid is first order with coexistence densities $\rho_{pI}R_p^3=0.46$ and $\rho_{pN}R_p^3=0.5$ according to a computer simulation [21]. The excess free energy density per volume can be expressed as

$$\frac{F_{ex}}{k_BTV}=\Phi_{s,b}-\rho_p\ln\alpha, \tag{28}$$

with

$$\frac{\alpha}{1-\eta_s}=\exp\left(-\frac{(\pi^2R_s^2R_p+2\pi R_p^2R_s)\rho_s}{1-\eta_s}-\frac{\pi^4R_s^4R_p^2\rho_s^2}{2(1-\eta_s)^2}\right), \tag{29}$$

where $\eta_s=4\pi R_s^3\rho_s/3$ is the packing fraction of the spheres and $\Phi_{s,b}$ is the excess free energy density of a pure hard sphere fluid. α can be considered as the free-volume fraction, i.e., the relative amount of the volume V that is accessible to the platelets. Besides providing access to inhomogeneous density distributions the above geometry-based density functional theory for mixtures of hard spheres and platelets offers in addition a systematic approach to calculate the work $W=-k_BT\ln\alpha$ required to insert a platelet into a solution of spheres. The expression for the free-volume fraction α in Eq. (29) is equivalent to the result from a recent scaled-particle approach [10]. For comparison we note that the corresponding free-volume fraction for thin rods is given by

$$\frac{\alpha}{1-\eta_s}=\exp\left(-\frac{\pi LR_s^2\rho_s}{1-\eta_s}\right). \tag{30}$$

From the bulk grand potential function all thermodynamic quantities can be calculated. Equating the pressure and the chemical potentials of both species in both phases yields the coexisting densities.

Figure 3(a) displays the calculated phase diagram for a binary mixture of spheres and thin platelets for size ratio $R_s/R_p=2$ as a function of the chemical potential μ_p of the platelets and the number density ρ_s of the spheres. The tie lines are horizontal because of the equality of μ_p of the coexisting phases. The binodal for coexisting states is shown, where a sphere-rich and a platelet-poor liquid phase coexists with a sphere-poor and a platelet-rich liquid phase. The coexistence region is bounded by a lower critical point below which only a single stable phase is found. For convenience we have introduced the dimensionless variable $\mu_p^*\equiv\mu_p-k_BT\ln(\Lambda_p^3/R_p^3)$, and dropped the star in order to avoid a clumsy notation. Figure 3(b) displays an alternative representation of the phase diagram in terms of the number densities of both species. The figure illustrates the fractionation of both spheres and platelets due to the phase transition. Upon increasing the size ratio the critical point shifts to larger densities of the spheres.

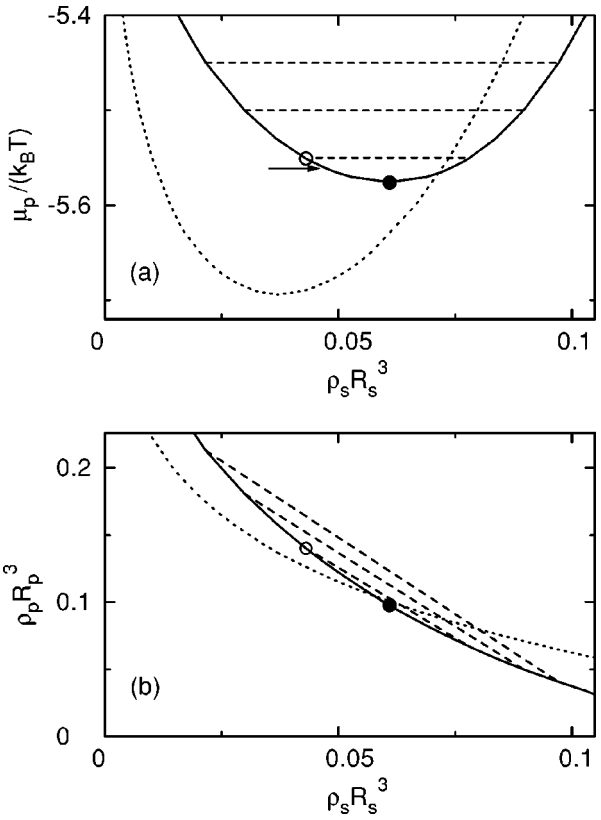

FIG. 3. (a) Bulk and surface phase diagrams of binary mixtures of hard spheres of radius R_s and thin hard platelets of radius $R_p=R_s/2$ as a function of the chemical potential of the platelets μ_p and the number density of the spheres ρ_s. The straight dashed lines are tie lines illustrating liquid-liquid phase coexistence. (b) Phase diagram of the same fluid in the density-density plane, where ρ_p is the number density of the platelets. In (a) and (b) the solid and open circles denote the bulk critical point and the wetting transition point, respectively. Between the wetting transition point and the critical point the sphere-rich liquid phase completely wets the interface between the hard wall and the sphere-poor liquid phase. The dotted curve is the binodal as calculated without the last term in parentheses on the RHS of Eq. (29) which is equivalent to the bulk phase diagram of a binary mixture of spheres of radius R_s and thin rods of length $L=2.07R_s$ (see the main text). In Fig. 4 density profiles near a hard wall are shown along the thermodynamic path indicated by the arrow at $\mu_p/(k_BT)=-5.56$ in (a); in (b) this path would run parallel to the dashed tie lines.

The dotted lines in Fig. 3 represent the binodal as calculated without the term proportional to ρ_s^2 in large parentheses on the right hand side (RHS) of Eq. (29) which is equivalent to considering a binary mixture of spheres and thin rods of length $L=\pi R_p+2R_p^2/R_s=2.07R_s$ as is apparent from a comparison of Eqs. (29) and (30). The phase boundaries and the lower critical point are shifted to smaller values of ρ_s. In other words, the number density of the spheres in the sphere-poor phase is increased by taking into account the last term in parentheses in Eq. (29). This term takes into account contributions from the third virial coefficient.

IV. BINARY SPHERE-PLATELET MIXTURE NEAR A PLANAR HARD WALL

The density profiles of both components of the binary mixture of hard spheres and thin platelets close to a planar hard wall are obtained by a numerical minimization of the grand potential functional (1) with the excess free energy functional given by Eq. (2). We fix the chemical potential μ_p of the platelets and approach the bulk phase boundary from the sphere-poor side. Upon decreasing μ_p the adsorption behavior changes qualitatively, and it is worthwhile to distinguish the following two cases. For $\mu_p/(k_BT)>-5.551$ we find that the wall is only partially wetted by the spheres. The layer thickness of the sphere-rich phase forming close to the wall increases continuously, but remains finite at coexistence. For $\mu_p/(k_BT)<-5.551$ we observe complete wetting. The transition to complete wetting appears to be first order because the excess adsorptions $\Gamma_l=R_l^2\int_0^\infty dz[\rho_l(z)-\rho_l(\infty)]$ with $l=p,r$, calculated along the coexistence curve jump to a macroscopic value upon approaching the wetting transition point. Figure 4(a) displays the sphere density profiles at $\mu_p/(k_BT)=-5.56$ signaling the growth of a thick layer of sphere liquid at the wall. The corresponding platelet profiles are shown in Fig. 4(b) and indicate how the platelets become more depleted as the sphere-rich layer grows. Upon approaching the chemical potential of the spheres at bulk coexistence $\mu_s/(k_BT)=11.298\,295$, the calculated density profiles at the liquid-liquid interface become virtually indistinguishable from the ones of the free liquid-liquid interface between coexisting bulk phases, and the layer thickness diverges logarithmically, as expected for the case of complete wetting in systems governed by short-ranged forces. With increasing chemical potential of the platelets, and hence increasing distance to the critical point [see Fig. 3(a)], the interface becomes sharper, i.e., it crosses over from one to the other limiting bulk value over a shorter distance. The wavelength $\lambda=1.76R_s$ of the oscillations of the density profiles close to the wall reflects the size of the spheres.

Similar to recent studies of wetting in sphere-polymer [3,5] and sphere-rod [4] mixtures, we have not been able to numerically resolve the prewetting line which should emerge tangentially from the coexistence curve at the wetting transition. In contrast to those studies there are no layering transitions in the partial wetting regime for the sphere-platelet mixture. This holds also for the aforementioned toy model without the last term in Eq. (4) which exhibits the same bulk phase diagram as the corresponding sphere-rod mixture (see the dotted curves in Fig. 3). Taking into account the weight function $w_2^{(p)}(z,\theta_p)$ [Eq. (16)] leads to wetting phenomena of sphere-platelet mixtures which are different from those of sphere-rod mixtures even if the bulk phase diagrams of both systems are identical. Finally, we note that the wetting behavior discussed above remains unchanged upon increasing the size ratio of the platelets and the spheres (e.g., $R_p>R_s/2$).

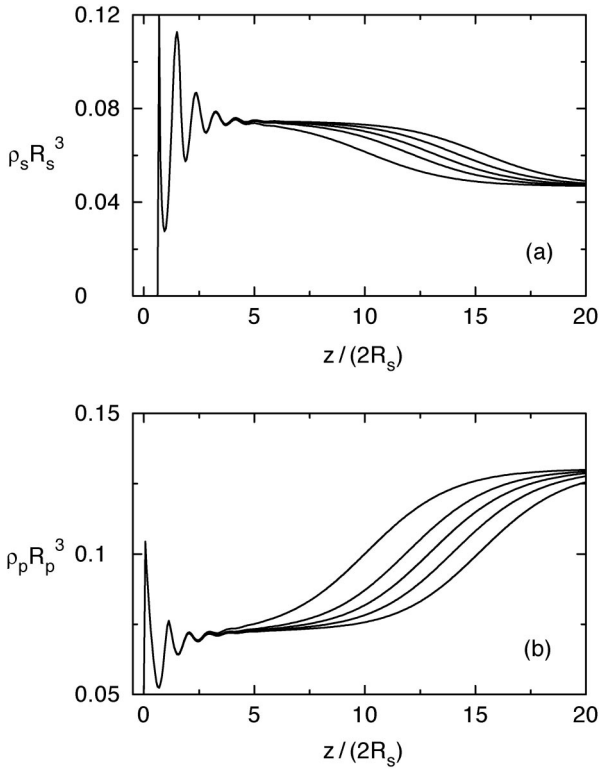

FIG. 4. Equilibrium density profiles of hard spheres of radius R_s (a) and thin hard platelets of radius $R_p=R_s/2$ (b) in contact with a planar hard wall at $z=0$ as the bulk phase boundary is approached along the path indicated by the arrow in Fig. 3(a). The chemical potentials of the spheres are $\mu_s/(k_BT)=11.298\,21$, 11.298 23, 11.298 25, 11.298 27, 11.298 29 corresponding to $\rho_s R_s^3=0.046\,719$, 0.046 725, 0.046 731, 0.046 737, 0.046 743 (from left to right) where the chemical potential at bulk coexistence is $\mu_s/(k_BT)=11.298\,295$ so that $\rho_s R_s^3=0.046\,744$. In (a) $\rho_s(z<R_s)=0$ and in (b) $\rho_p(z<0)=0$; the contact values at $z=R_s$ and $z=0$, respectively, are not shown on the present scales.

V. SUMMARY

We have developed a geometry-based density functional theory for fluids consisting of hard spheres and thin platelets in the limit of low platelet concentration. The bulk and surface phase diagram and the density profiles near a planar hard wall are determined numerically with the following main results.

(1) Figure 1 illustrates that from their side view thin platelets may be regarded as thin rods and from their top view as two-dimensional spheres. On the basis of this consideration we have shown that the geometry-based density functional

theory developed for binary mixture of hard spheres and thin rods [13–16] can be consistently extended to the problem of hard spheres mixed with thin hard platelets in the limit of low platelet concentration by introducing an additional weight function which characterizes the surface of a platelet. The volume accessible to a thin platelet of radius R_p in the presence of a sphere is smaller than the corresponding one of a thin rod of length $L=2R_p$ because of the extended surface of the platelet (Fig. 2).

(2) The bulk phase diagram exhibits two-phase coexistence between sphere-rich and sphere-poor phases which is bounded by a lower critical point below which a single stable phase is found (Fig. 3). The phase boundaries and the critical point of the corresponding phase diagram for a binary mixture of hard spheres and thin rods are shifted to smaller values of the density of the spheres due to smaller intermolecular interactions between thin rods and spheres as compared with those between thin platelets and spheres.

(3) For the mixture near a planar hard wall, a first-order wetting transition by the sphere-rich phase occurs. In the partial wetting regime no layering transitions are found in contrast to recent studies on binary mixtures of spheres and nonadsorbing polymers or thin hard rods.

We have focused on the case of noninteracting platelets as regards their mutual interactions, which constitutes a minimal model for nonspherical particles with nonvanishing surface area. With increasing density of the platelets, interactions between platelets must be included [22,23]. The consistent treatment of these nontrivial platelet-platelet interactions within a geometry-based density functional theory remains as a challenge.

ACKNOWLEDGMENT

The authors thank R. Roth for useful discussions.

APPENDIX: EVALUATION OF MAYER FUNCTIONS

1. Sphere-platelet Mayer function

Without loss of generality we take the difference vector between the centers of mass of the platelet and the sphere to lie in the equatorial plane: $\mathbf{r}=(r\cos\phi, r\sin\phi, 0)$. Due to rotational symmetry, we can choose the platelet normal to be aligned parallel to the x axis: $\theta_p=\pi/2$ and $\phi_p=0$. First, we determine the limiting distance $r_{lim}(\phi)$ between the centers of mass of the platelet and the sphere for which the platelet just touches the outside of the sphere. As is illustrated in Fig. 5, there are two different ways in which a platelet can touch the outside of a sphere: when the platelet is close to the sphere it will touch the sphere tangentially with its face [Fig. 5(a)] whereas when it is sufficiently far from the surface, its rim touches the sphere [Fig. 5(b)]. The crossover between these two regimes occurs at

$$\phi_c = \arccos\left(\frac{R_s}{\sqrt{R_s^2+R_p^2}}\right). \tag{A1}$$

A straightforward geometrical reasoning yields

$$r_{lim}(\phi) = \begin{cases} \dfrac{R_s}{|\cos\phi|}, & \phi \in [0,\phi_c]\cup[\pi-\phi_c,\pi+\phi_c]\cup[2\pi-\phi_c,2\pi], \\ R_p|\sin\phi| + \sqrt{R_s^2 - R_p^2\cos^2\phi}, & \phi\in[\phi_c,\pi-\phi_c]\cup[\pi+\phi_c,2\pi-\phi_c]. \end{cases} \tag{A2}$$

The Mayer function of the interaction potential between a hard sphere and a thin platelet is given by

$$-f_{sp}(r,\phi) = \Theta(r_{lim}(\phi)-r) = \frac{1}{2}[g_+(r,\phi)+g_-(r,\phi)+h_+(r,\phi)+h_-(r,\phi)], \tag{A3}$$

with

$$g_\pm(r,\phi) = \Theta(R_s^2 - r^2 - R_p^2 \pm 2rR_p\sin\phi) \tag{A4}$$

and

$$h_\pm(r,\phi) = \Theta(R_s - |r\cos\phi|)\times\Theta(R_p - |r\sin\phi \pm \sqrt{R_s^2 - r^2\cos^2\phi}|). \tag{A5}$$

The function $g_+(r,\phi)+g_-(r,\phi)$ counts the number of end points (0,1,2) of the projection of the rim of a platelet on the x-y plane that are inside the sphere. In Eq. (A5), the first Heaviside function is nonzero only if the plane defined by the platelet intersects the sphere. If it does, the function $h_+(r,\phi)+h_-(r,\phi)$ counts how often (0,1,2) the projection of a platelet on the x-y plane intersects the surface of the sphere.

An alternative representation of the Mayer function is given by the spatial convolution

$$-f_{sp}(r,\phi) = \int_0^\infty dr_1 \int_0^{2\pi} d\phi_1 \int_0^\pi d\theta_1 r_1^2 \times\sin\theta_1[A_1(\mathbf{r}-\mathbf{r}_1)B_1(\mathbf{r}_1) + A_2(\mathbf{r}-\mathbf{r}_1)B_2(\mathbf{r}_1)] \tag{A6}$$

with

$$A_1(\mathbf{r}) = \frac{1}{2}[\delta(\mathbf{r}+\mathbf{e}R_p) + \delta(\mathbf{r}-\mathbf{e}R_p)], \tag{A7}$$

$$A_2(\mathbf{r}) = \frac{1}{4}\int_{-R_p}^{R_p} dl\ \delta(\mathbf{r}+\mathbf{e}l), \tag{A8}$$

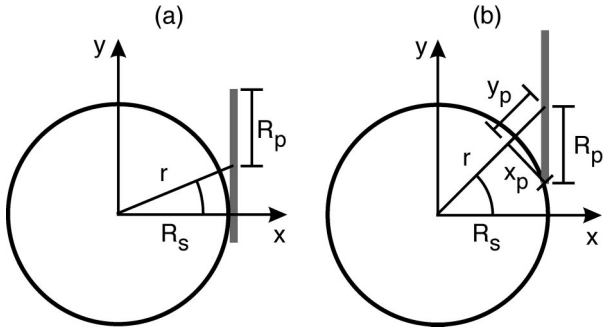

FIG. 5. Geometries relevant for the determination of the limiting distance $r=|\mathbf{r}|=r_{lim}(\phi)$ between the centers of mass of a thin platelet of radius R_p and a sphere of radius R_s for which the platelet just touches the outside of the sphere. For the evaluation of the sphere-platelet Mayer function the coordinate system is chosen such that the x axis is parallel to the normal of the platelet $\boldsymbol{\omega}_p$. The z axis and the y axis are parallel to the vectors $\boldsymbol{\omega}_p\times\mathbf{r}$ and $(\boldsymbol{\omega}_p\times\mathbf{r})\times\boldsymbol{\omega}_p$, respectively, where $\mathbf{r}$ is the interparticle vector. The z axis is perpendicular to the plane of the figure. The projection of a sphere of radius R_s on the x-y plane is a circular area, while the projection of a *circular* platelet of radius R_p on the x-y plane is a line segment of length $2R_p$ which is oriented parallel to the y axis. Equation (A2) can be derived using $x_p=R_p\cos\phi$ and $y_p=R_p\sin\phi$. The platelet touches the sphere tangentially with its face in (a), but with its rim in (b). Only the projections of the platelets and spheres on the plane of the figure are shown.

$$B_1(\mathbf{r}) = \Theta(R_s - |\mathbf{r}|), \tag{A9}$$

$$B_2(\mathbf{r}) = 2\delta(R_s - |\mathbf{r}|)\frac{|\mathbf{r}\cdot\mathbf{e}|}{|\mathbf{r}|}, \tag{A10}$$

where $\mathbf{e}=(0,1,0)$ and $\mathbf{r}_1=r_1(\sin\theta_1\cos\phi_1,\sin\theta_1\sin\phi_1,\cos\theta_1)$. The evaluation of the integrals in Eq. (A6) is straightforward. We emphasize that the Mayer function $f_{sp}(r,\phi)$ is *identical* to the Mayer function of the interaction potential between a hard sphere and a thin rod of length $L=2R_p$ which is oriented parallel to the y axis: $\theta_r=\pi/2$ and $\phi_r=\pi/2$ (see Ref. [16] and in particular Appendix A 1 therein). However, spatial integrals of the sphere-platelet and sphere-rod Mayer functions are *qualitatively different* as is discussed in Sec. II of the main text and in the following section.

2. Integral of sphere-platelet Mayer function

In order to calculate the integral of the sphere-platelet Mayer function we take the difference vector between the centers of mass of the platelet and the sphere to be $\mathbf{r}=(\rho\sin\phi,\rho\cos\phi,z)$. Due to rotational symmetry around the z axis, we can choose the platelet normal to be aligned in the x-z plane so that $\phi_p=0$. Using Eq. (A3) the integral of the Mayer function reads

$$l_{sp}(z,\theta_p) = -\int_{-\infty}^{\infty}dx\int_{-\infty}^{\infty}dy\, f_{sp}(x,y,z,\omega_p) = \int_0^{2\pi}d\phi\int_0^{\infty}d\rho\,\rho\Theta(r_{lim}(\phi')-r) \tag{A11}$$

with

$$\phi' = \arccos\left[\frac{z\cos\theta_p+\rho\cos\phi\sin\theta_p}{\sqrt{\rho^2+z^2}}\right]. \tag{A12}$$

The corresponding integral of the sphere-rod Mayer function is given by

$$l_{sr}(z,\theta_r) = -\int_{-\infty}^{\infty}dx\int_{-\infty}^{\infty}dy\, f_{sr}(x,y,z,\omega_r) = \int_0^{2\pi}d\phi\int_0^{\infty}d\rho\,\rho\Theta(r_{lim}(\phi')-r) \tag{A13}$$

with

$$\phi' = \arcsin\left[\frac{z\cos\theta_r+\rho\cos\phi\sin\theta_r}{\sqrt{\rho^2+z^2}}\right]. \tag{A14}$$

For the cases $\theta_p=0$ and $\theta_r=\pi/2$ the integrals in Eqs. (A11) and (A13) can be calculated easily leading to Eqs. (24)–(27). Alternative representations are given by the spatial convolutions

$$\begin{aligned} l_{sp}(z,\theta_p=0) &= \int_{-\infty}^{\infty}dz_1[w_0^{(p)}(z_1,0)w_3^{(s)}(z-z_1) \\ &\quad + w_1^{(p)}(z_1,0)w^{(sp)}(z-z_1,0) + w_2^{(p)}(z_1,0)w_1^{(s)}(z-z_1)] \\ &= p_1(z)+p_2(z)+p_3(z) \end{aligned} \tag{A15}$$

and

$$\begin{aligned} l_{sr}\left(z,\theta_r=\frac{\pi}{2}\right) &= \int_{-\infty}^{\infty}dz_1\left[w_0^{(r)}\left(z_1,\frac{\pi}{2}\right)w_3^{(s)}(z-z_1)\right. \\ &\quad \left. + w_1^{(r)}\left(z_1,\frac{\pi}{2}\right)w^{(sr)}\left(z-z_1,\frac{\pi}{2}\right)\right] \\ &= r_1(z)+r_2(z) \end{aligned} \tag{A16}$$

with

$$w_2^{(p)}(z,0) = 2\pi R_p^2\delta(z) = 8R_p w_1^{(p)}(z,0) = 2\pi R_p^2 w_0^{(p)}(z,0), \tag{A17}$$

$$\begin{aligned} w_3^{(s)}(z) &= \pi(R_s^2-z^2)\Theta(R_s-|z|) = 2\pi(R_s^2-z^2)w_1^{(s)}(z) \\ &= \frac{\pi}{8}\sqrt{R_s^2-z^2}\,w^{(sp)}(z,0) = \frac{\pi}{8}\sqrt{R_s^2-z^2}\,w^{(sr)}\left(z,\frac{\pi}{2}\right), \end{aligned} \tag{A18}$$

$$w_1^{(r)}\left(z,\frac{\pi}{2}\right) = \frac{L}{4}\delta(z) = \frac{L}{4}w_0^{(r)}\left(z,\frac{\pi}{2}\right). \tag{A19}$$

Figure 6 displays the integrals of the sphere-platelet and sphere-rod Mayer functions $l_{sp}(z,\theta_p=0)$ and $l_{sr}(z,\theta_r=\pi/2)$ together with the contributions $p_1(z),p_2(z),p_3(z)$ and

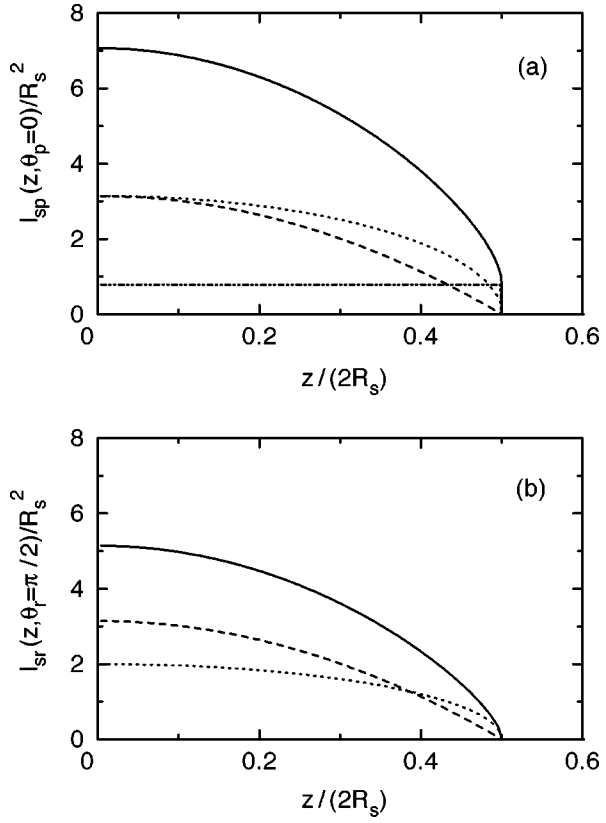

FIG. 6. Integral of the sphere-platelet Mayer function $l_{sp}(z,\theta_p=0)=p_1(z)+p_2(z)+p_3(z)$ for size ratio $R_p=R_s/2$ in (a) and integral of the sphere-rod Mayer function $l_{sr}(z,\theta_r=\pi/2)=r_1(z)+r_2(z)$ for size ratio $L=R_s$ in (b) as obtained from Eqs. (A15) and (A16) (solid lines). The dashed, dotted, and dash-dotted lines represent the contributions $p_1(z)=\pi(R_s^2-z^2)\Theta(R_s-|z|)$, $p_2(z)=2\pi R_p\sqrt{R_s^2-z^2}\Theta(R_s-|z|)$, and $p_3(z)=\pi R_p^2\Theta(R_s-|z|)$ in (a) [see Eqs. (A15), (A17), and (A18)]. In (b) the dashed and dotted lines represent the contributions $r_1(z)=p_1(z)$ and $r_2(z)=2L\sqrt{R_s^2-z^2}\Theta(R_s-|z|)$, respectively [see Eqs. (A16), (A18), and (A19)]. All functions are divided by R_s^2.

$r_1(z), r_2(z)$ for the size ratio $R_p=R_s/2=L/2$. The corresponding schematic illustrations of the steric interactions of the sphere with the platelet and rod, respectively, are shown in Fig. 2. The term $p_3(z)$ takes into account the contribution due to the surface of the platelet. There is no corresponding contribution $r_3(z)$ to the integral of the sphere-rod Mayer function since the surface of thin rods is negligibly small.

The second virial coefficients for the homogeneous and isotropic bulk fluids are given by

$$B_{sp}=\int dz\, l_{sp}(z,\theta_p=0)=\zeta_0^{(p)}\zeta_3^{(s)}+\zeta_1^{(p)}\zeta_2^{(s)}+\zeta_2^{(p)}\zeta_1^{(s)} \quad \text{(A20)}$$

$$=\frac{4\pi}{3}R_s^3+\pi^2R_s^2R_p+2\pi R_sR_p^2 \quad \text{(A21)}$$

and

$$B_{sr}=\int dz\, l_{sp}\left(z,\theta_r=\frac{\pi}{2}\right)=\zeta_0^{(r)}\zeta_3^{(s)}+\zeta_1^{(r)}\zeta_2^{(s)}=\frac{4\pi}{3}R_s^3+\pi R_s^2L. \quad \text{(A22)}$$

Here the weight functions are linked with a geometrical representation of the particles which is given in terms of fundamental measures defined as $\zeta_\lambda^{(j)}=\int dz\, w_\lambda^{(j)}$, where $j=s,p,r$ labels the species, and $\lambda=0,1,2,3$ corresponds to the Euler characteristic, integral mean curvature, surface, and volume of the particles. We note that the values of B_{sp} and B_{sr} are independent of θ_p and θ_r, respectively. The second virial coefficients are related to the surface tension of ideal gases of platelets and rods outside a spherical surface of radius R_s according to

$$\frac{\gamma_{id}^{(p)}(R_s)}{\rho_pk_BT}=\frac{1}{4\pi R_s^2}\left(B_{sp}-\frac{4\pi}{3}R_s^3\right)=\frac{\pi R_p}{4}+\frac{R_p^2}{2R_s} \quad \text{(A23)}$$

and

$$\frac{\gamma_{id}^{(r)}(R_s)}{\rho_pk_BT}=\frac{1}{4\pi R_s^2}\left(B_{sr}-\frac{4\pi}{3}R_s^3\right)=\frac{L}{4}. \quad \text{(A24)}$$

In contrast to earlier statements in Refs. [24,25] the surface tension of an ideal gas of thin platelets *depends* on the radius R_s of the sphere whereas the corresponding surface tension of an ideal gas of thin rods is *independent* of R_s, despite the fact that the sphere-platelet and sphere-rod Mayer functions are the same apart from a different definition of the angle ϕ in Eqs. (A1)–(A5). The dependence of the surface tension on the radius of the spherical surface is of considerable importance for the so-called Helfrich expansion of the surface free energy of arbitrarily curved surfaces in terms of powers of the principal curvatures [26].

Based on the discussion of the limiting cases $\theta_p=0$ and $\theta_r=\pi/2$ the meaning of the weight functions for arbitrary values of θ_p and θ_r defined in Eqs. (15), (16), and (19)–(21) can easily be inferred. For example, the Heaviside step function in

$$w_2^{(p)}(z,\theta_p)=\frac{\pi R_p}{\sin\theta_p}\Theta(R_p\sin\theta_p-|z|) \quad \text{(A25)}$$

characterizes the projection of the surface of a platelet on the z axis for a given angle θ_p between the normal of the platelet and the z axis (see Fig. 1). The prefactor $\pi R_p/\sin\theta_p$ ensures that the integral $\zeta_2^{(p)}=\int dz\, w_2^{(p)}(z,\theta_p)$ yields the correct fundamental measure, namely, the surface area of a platelet. The necessity for including the weight functions $w^{(sp)}(z,\theta_p)$ and $w^{(sr)}(z,\theta_r)$, which contain informations about *both* species of the binary mixture, follows from the decompositions of the integrals of the Mayer functions in Eqs. (18) and (23). The remaining functions $v^{(sp)}(z,\theta_p)$ and $v^{(sr)}(z,\theta_r)$ in Eqs. (17) and (22), respectively, can be determined numerically. An analytic expression for $v^{(sr)}(z,\theta_r)$ has been derived in Appendix B 2 in Ref. [16]. The integral $\zeta_2^{(s)}=\int dz\, w^{(sp)}\times(z,\theta_p)=\int dz\, w^{(sr)}(z,\theta_r)$ yields the surface of a sphere of radius R_s.

[1] W. C. K. Poon, P. N. Pusey, and H. N. W. Lekkerkerker, Phys. World **9**, 27 (1996).
[2] M. Adams, Z. Dogic, S. L. Keller, and S. Fraden, Nature (London) **393**, 349 (1998).
[3] J. M. Brader, R. Evans, M. Schmidt, and H. Löwen, J. Phys.: Condens. Matter **14**, L1 (2002).
[4] R. Roth, J. M. Brader, and M. Schmidt, Europhys. Lett. **63**, 549 (2003).
[5] M. Dijkstra and R. van Roij, Phys. Rev. Lett. **89**, 208303 (2002).
[6] M. Piech and J. Y. Walz, J. Colloid Interface Sci. **232**, 86 (2000).
[7] S. M. Oversteegen and H. N. W. Lekkerkerker, Phys. Rev. E **68**, 021404 (2003).
[8] L. Harnau and S. Dietrich, Phys. Rev. E **69**, 051501 (2004).
[9] S. M. Oversteegen and H. N. W. Lekkerkerker, Physica A **341**, 23 (2004).
[10] S. M. Oversteegen and H. N. W. Lekkerkerker, J. Phys. Chem. **120**, 2470 (2004).
[11] T. G. Mason, Phys. Rev. E **66**, 060402(R) (2002).
[12] G. C. Maitland, Curr. Opin. Colloid Interface Sci. **5**, 301 (2000).
[13] M. Schmidt, Phys. Rev. E **63**, 050201 (2001).
[14] M. Schmidt and C. von Ferber, Phys. Rev. E **64**, 051115 (2001).
[15] M. Schmidt and A. R. Denton, Phys. Rev. E **65**, 021508 (2002).
[16] J. M. Brader, A. Esztermann, and M. Schmidt, Phys. Rev. E **66**, 031401 (2002).
[17] Y. Rosenfeld, Phys. Rev. Lett. **63**, 980 (1989).
[18] P. Tarazona, Phys. Rev. Lett. **84**, 694 (2000).
[19] R. Roth, R. Evans, A. Lang, and G. Kahl, J. Phys.: Condens. Matter **14**, 12063 (2002).
[20] Y. Rosenfeld, Phys. Rev. E **50**, R3318 (1994).
[21] M. A. Bates, J. Chem. Phys. **111**, 1732 (1999).
[22] L. Harnau, D. Costa, and J.-P. Hansen, Europhys. Lett. **53**, 729 (2001).
[23] L. Harnau and S. Dietrich, Phys. Rev. E **65**, 021505 (2002).
[24] K. Yaman, P. Pincus, and C. M. Marques, Phys. Rev. Lett. **78**, 4514 (1997).
[25] K. Yaman, M. Jeng, P. Pincus, C. Jeppesen, and C. M. Marques, Physica A **247**, 159 (1997).
[26] W. Helfrich, Z. Naturforsch. C **28**, 693 (1973).